# Inside-out regulation of E-cadherin conformation and adhesion

Ramesh Koirala[a,b,1], Andrew Vae Priest[a,b,1], Chi-Fu Yen[b], Joleen S. Cheah[a], Willem-Jan Pannekoek[c], Martijn Gloerich[c], Soichiro Yamada[a], and Sanjeevi Sivasankar[a,2]

[a]Department of Biomedical Engineering, University of California, Davis, CA 95616; [b]Department of Physics and Astronomy, Iowa State University, Ames, IA 50011; and [c]Molecular Cancer Research, Center for Molecular Medicine, University Medical Center Utrecht, 3584 CG Utrecht, The Netherlands

Edited by Barry Honig, Columbia University, New York, NY, and approved June 21, 2021 (received for review March 2, 2021)

**Cadherin cell–cell adhesion proteins play key roles in tissue morphogenesis and wound healing. Cadherin ectodomains bind in two conformations, X-dimers and strand-swap dimers, with different adhesive properties. However, the mechanisms by which cells regulate ectodomain conformation are unknown. Cadherin intracellular regions associate with several actin-binding proteins including vinculin, which are believed to tune cell–cell adhesion by remodeling the actin cytoskeleton. Here, we show at the single-molecule level, that vinculin association with the cadherin cytoplasmic region allosterically converts weak X-dimers into strong strand-swap dimers and that this process is mediated by myosin II–dependent changes in cytoskeletal tension. We also show that in epithelial cells, ∼70% of apical cadherins exist as strand-swap dimers while the remaining form X-dimers, providing two cadherin pools with different adhesive properties. Our results demonstrate the inside-out regulation of cadherin conformation and establish a mechanistic role for vinculin in this process.**

inside-out regulation | conformation | E-cadherin | ectodomain | vinculin

E-cadherins (Ecads) are essential, calcium-dependent cell–cell adhesion proteins that play key roles in the formation of epithelial tissue and in the maintenance of tissue integrity. Ecad adhesion is highly plastic and carefully regulated to orchestrate complex movement of epithelial cells, and dysregulation of adhesion is a hallmark of numerous cancers (1). However, little is known about how cells dynamically regulate the biophysical properties of individual Ecads.

The extracellular region of Ecads from opposing cells bind in two distinct *trans* orientations: strand-swap dimers and X-dimers (Fig. 1 *A* and *B*). Strand-swap dimers are the stronger cadherin adhesive conformation and are formed by the exchange of conserved tryptophan (Trp) residues between the outermost domains of opposing Ecads (2–4). In contrast, X-dimers, which are formed by extensive surface interactions between opposing Ecads, are a weaker adhesive structure and serve as an intermediate during the formation and rupture of strand-swap dimers (5–7). Using cell-free, single-molecule experiments we previously showed that X-dimers and strand-swap dimers can be distinguished based on their distinctly different response to mechanical force. When a strand-swap dimer is pulled, its lifetime decreases with increasing force, resulting in the formation of a slip bond (8, 9) (Fig. 1*B*). In contrast, an X-dimer responds to pulling force by forming a catch bond, where bond lifetime initially increases up to a threshold force and then subsequently decreases (8, 10) (Fig. 1*B*). It has also been shown that wild-type Ecad ectodomains in solution can interconvert between X-dimer and strand-swap dimer conformations (9, 11). However, the biophysical mechanisms by which Ecad conformations (and adhesion) are regulated on the cell surface are unknown.

The cytoplasmic region of Ecad associates with the catenin family of proteins, namely, p120-catenin, β-catenin, and α-catenin. The Ecad–catenin complex, in turn, links to filamentous actin (F-actin) either by the direct binding of α-catenin and F-actin or by the indirect association of α-catenin and F-actin via vinculin (12) (Fig. 1*A*). Adhesive forces transmitted across intercellular junctions by Ecad induce conformational changes in α-catenin (13, 14), strengthen F-actin binding (15), and recruit vinculin to the sites of force application (16, 17). However, vinculin and α-catenin do not merely serve as passive cytoskeletal linkers; they also dynamically modulate cytoskeletal rearrangement and recruit myosin to cell–cell junctions (13, 18–20). Studies show that α-catenin and vinculin play important roles in strengthening and stabilizing Ecad adhesion: bead-twisting experiments show force-induced stiffening of Ecad-based junctions and cell doublet stretching experiments demonstrate reinforcement of cell–cell adhesion in vinculin- and α-catenin–dependent manners (18, 19, 21).

Currently, actin anchorage and cytoskeletal remodeling are assumed to be the exclusive mechanisms by which α-catenin and vinculin strengthen Ecad adhesion (22–24). Here, we directly map the allosteric effects of cytoplasmic proteins on Ecad ectodomain conformation and demonstrate, at the single-molecule level, that vinculin association with the Ecad cytoplasmic region switches X-dimers to strand-swap dimers. We show that cytoskeletal tension, due to vinculin-mediated recruitment of myosin II, regulates Ecad ectodomain structure and adhesion. Finally, we demonstrate that only ∼50% of Ecads are linked to the underlying cytoskeleton and that while about 70% of Ecads form strand-swap dimers the remaining form X-dimers, which provides cells with two Ecad pools with different adhesive properties.

## Significance

Cadherin cell–cell adhesion proteins play key roles in the formation and maintenance of tissues. Their adhesion is carefully regulated to orchestrate complex movement of cells. While cadherin ectodomains bind in two conformations with different adhesive properties, the mechanisms by which cells regulate the conformation (and consequently adhesion) of individual cadherins are unknown. Here, we demonstrate that the association of intracellular vinculin with the cadherin cytoplasmic region regulates cadherin adhesion by switching ectodomains from a weak binding to the strongly adhesive conformation. In contrast to the prevailing view which suggests that vinculin regulates adhesion solely by remodeling the cytoskeleton, we show that vinculin can directly modulate single cadherin ectodomain conformation and this process is mediated by changes in cytoskeletal tension.

Author contributions: R.K., A.V.P., and S.S. designed research; R.K., A.V.P., C.-F.Y., and W.-J.P. performed research; J.S.C., M.G., and S.Y. contributed new reagents/analytic tools; R.K., A.V.P., C.-F.Y., W.-J.P., M.G., and S.S. analyzed data; and R.K., A.V.P., and S.S. wrote the paper.

The authors declare no competing interest.

This article is a PNAS Direct Submission.



[1]R.K. and A.V.P. contributed equally to this work.

[2]To whom correspondence may be addressed. Email: ssivasankar@ucdavis.edu.

This article contains supporting information online at https://www.pnas.org/lookup/suppl/doi:10.1073/pnas.2104090118/-/DCSupplemental.

Published July 22, 2021.

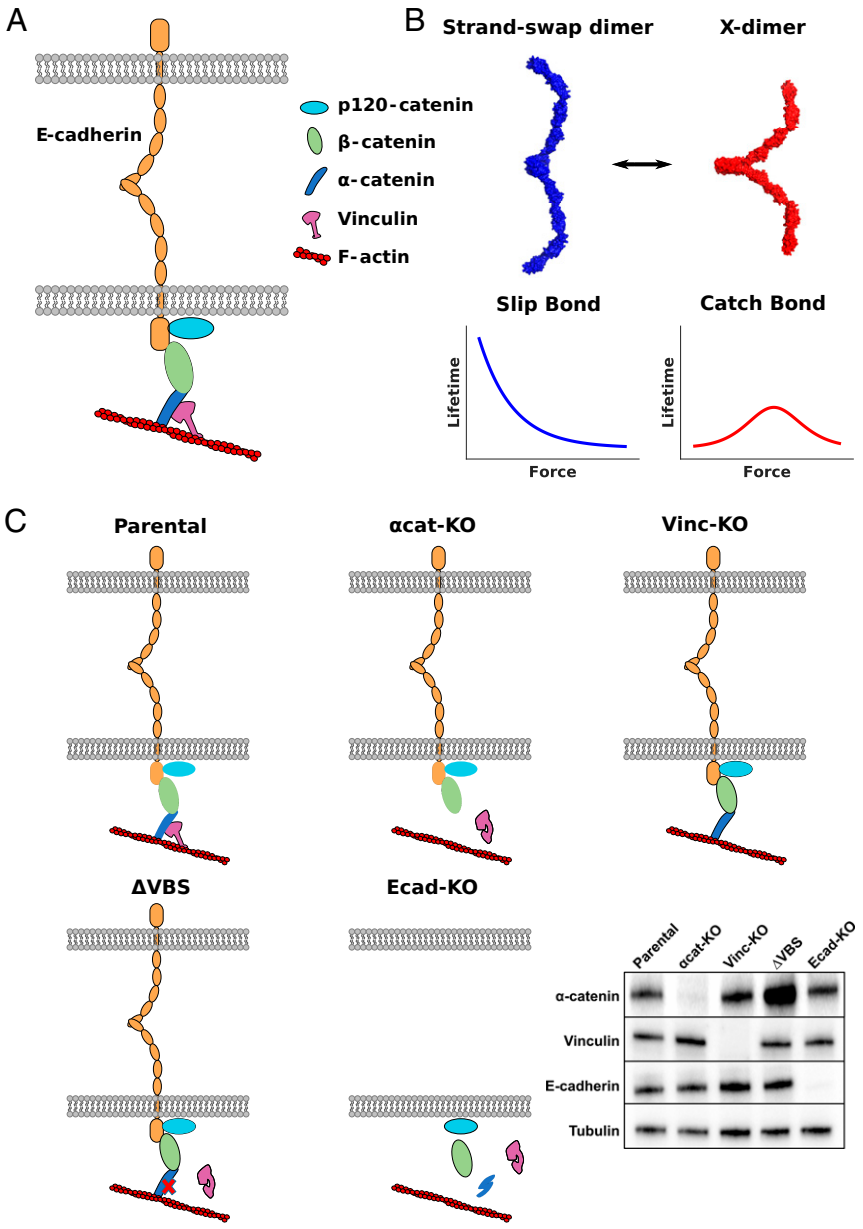


**Fig. 1.** Overview of experiment. (*A*) The extracellular region of Ecad from opposing cells mediates adhesion. The cytoplasmic region of Ecad associates either directly or indirectly with p120 catenin, β-catenin, α-catenin, vinculin, and F-actin. (*B*) Strand-swap dimers form slip bonds (blue) and X-dimers form catch bonds (red). Ecads interconvert between these two dimer conformations. Structures were generated from the crystal structure of mouse Ecad (PDB ID code 3Q2V); the X-dimer was formed by alignment to an X-dimer crystal structure (PDB ID code 3LNH). (*C*) Graphics showing the cell lines used in experiments and Western blot analysis of corresponding cell lysates.

## Results

**Single-Molecule Atomic Force Microscope (AFM) Measurements of Specific Ecad *Trans* Adhesion.** We measured interactions between recombinant Ecad extracellular regions immobilized on AFM cantilevers and Ecad endogenously expressed on the apical surface of confluent Madin–Darby canine kidney (MDCK) cell monolayers (Fig. 2*A*). To ensure that we measured single Ecad unbinding events, we immobilized Ecad on the AFM tip at low density and pressed on the cell surface with a low initial contact force (mean pressing force = 59 pN; *SI Appendix*, Fig. S1). Poisson statistics predict that even the maximum event rate we measure (19%; Fig. 2*B*) corresponds to ~90% probability of measuring single-molecule events.

Our experiments were performed with the following MDCK cells (Fig. 1*C*): parental cells (parental), vinculin knockout cells (vinc-KO), α-catenin knockout cells (αcat-KO) (25), αcat-KO cells rescued with α-catenin lacking the vinculin binding site (ΔVBS) (26), and Ecad knockout cells (Ecad-KO). We also performed measurements with parental cells in the presence of free tryptophan (parental-Trp) in order to trap Ecad in an X-dimer conformation (8). Additionally, we performed experiments in the presence of blebbistatin (parental-Bleb) in order to reduce myosin II–dependent cytoskeletal contractility. We quantified the specific and nonspecific binding rates for every cell line by measuring single unbinding events using either AFM tips that were decorated with Ecad (specific binding) or AFM tips that lacked Ecad (nonspecific binding). All cell lines, except Ecad-KO, showed a

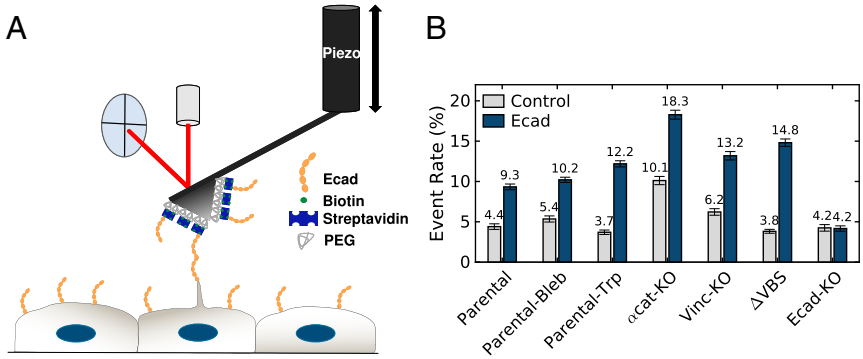


**Fig. 2.** Measuring specific and nonspecific interaction using AFM. (*A*) Biotinylated Ecad monomers were immobilized on AFM cantilevers functionalized with PEG and streptavidin as described in *Methods*. Interactions between Ecads on the cantilever and Ecads expressed on the apical surface of MDCK cells were measured. (*B*) Binding probabilities were measured using AFM cantilevers lacking Ecad (control experiment, light gray) or AFM cantilevers decorated with Ecad (Ecad, dark blue). Total numbers of Ecad/control measurements performed on each cell line were 6,793/3,361 measurements on parental cells, 8,593/3,719 measurements on parental-Bleb, 7,268/4,858 measurements on parental-Trp, 4,291/3,666 measurements on vinc-KO cells, 4,518/3,381 measurements on αcat-KO cells, 6,124/6,070 measurements on ΔVBS cells, and 3,672/2,449 measurements on Ecad-KO cells. Error bars are bootstrapped SDs.

significant increase in single unbinding events when the AFM tips were decorated with Ecad (Fig. 2*B*). In contrast, in the Ecad-KO cells, event rates using AFM tips with or without Ecad were similar to each other and were comparable to the nonspecific event rates measured with the other cell lines (Fig. 2*B*). Taken together, this confirmed that the measured specific events corresponded to Ecad–Ecad binding interactions.

Ecad conformation and cytoskeletal linkage in each cell line were determined from previously reported "signatures" in the measured force curves. Since force measurements have shown that pulling on a cell surface protein that is not linked to the cytoskeleton results in the formation of a membrane tether (27, 28) (Fig. 3*A*), we used membrane tethers to identify Ecads that are uncoupled from the actin cytoskeleton (Fig. 3*B*). Previous studies have also shown that pulling on a transmembrane protein that is firmly bound to the underlying cytoskeleton results in a linearly elastic response to pulling force (29, 30) (Fig. 3*C*). Since these jump events occur when interactions between proteins on the AFM tip and cell surface are weaker than the protein–cytoskeleton linkage, we interpreted jumps as a signature of actin-linked Ecads that form weak *trans* dimers, which rupture before failure of the Ecad–cytoskeletal linkage (Fig. 3*D*). Finally, if the Ecad *trans* dimers adhere robustly compared to the Ecad–cytoskeletal linkage, an initial steep increase in force is measured which relaxes viscoelastically when the Ecad–cytoskeletal bond ruptures, resulting in the formation of a cyto tether (Fig. 3 *E* and *F*). To further validate tether formation, we fit the membrane-tether and cyto-tether force-extension curves to the standard linear solid (SLS) model (*SI Appendix*, *Note 1*) (31). The SLS fitting parameters we obtained for the tethers were consistent with previous values obtained for tether formation on Jurkat cells and T cells (*SI Appendix*, Table S1) (31, 32).

**About 50% of Nonjunctional Ecads Are Coupled to the Actin Cytoskeleton.** We first compared the fraction of Ecad uncoupled from the cytoskeleton (membrane tethers) to the fraction of Ecads that are coupled to cortical actin (cyto tethers and jumps). Our data showed that in parental cells 55% ± 9% of Ecad on the apical surface of the cell are uncoupled from the actin cytoskeleton (Fig. 4*A*). Since α-catenin is believed to be vital in mediating Ecad linkage to F-actin, we next measured the cytoskeletal linkage of Ecad in αcat-KO cells. As anticipated from previous biochemical and cell biological results (33, 34), our data showed that the vast majority of Ecads (92% ± 12%) in αcat-KO cells are uncoupled from the actin cytoskeleton (Fig. 4*A*). In contrast, the fraction of uncoupled Ecads in both vinc-KO and ΔVBS cells, where Ecads are presumably weakly linked to F-actin by α-catenin, but where this linkage is not reinforced by vinculin (13, 35), was comparable to parental cells (65% ± 9% for vinc-KO and 45% ± 4% for ΔVBS cells; Fig. 4*A*). Taken together, these data confirm the obligatory role of α-catenin in mediating Ecad linkage to F-actin. These direct, single-molecule measurements of Ecad–actin coupling on the apical surface of live cells are in excellent agreement with previous single particle tracking of Ecad on the cell surface that inferred ~50% of Ecads on the apical surface of cells are coupled to the actin cytoskeleton (36).

**Absence of Vinculin Binding Weakens Adhesion of Individual Ecads.** We next compared the fraction of weak (jumps) and strong (cyto tethers) *trans* dimers formed by cytoskeleton-coupled Ecad. Our data showed that in parental cells that contain both α-catenin and vinculin, 77% ± 16% of cytoskeleton-coupled Ecads bind robustly while the remaining 23% ± 14% of Ecads interact weakly (Fig. 4*B*). In contrast, in vinc-KO cells, only 5% ± 3% of cytoskeleton-coupled Ecads bind strongly (Fig. 4*B*). Similarly, in ΔVBS cells where vinculin cannot bind to α-catenin, only 2% ± 1% of cytoskeleton-linked Ecads bind in a robust binding conformation (Fig. 4*B*). Taken together, this indicates that vinculin association with the Ecad cytoplasmic region is required for robust Ecad *trans* dimerization. It is important to point out that the strength of *trans* dimer adhesion in the absence of α-catenin could not be determined by comparing the fraction of cyto tethers and jumps because these events were extremely rare in the αcat-KO cells.

Since an Ecad *trans* dimer can exist in two different conformations with different adhesive strengths—weaker X-dimer and stronger strand-swap dimer—we asked whether the weak (jumps) and strong (cyto tethers) adhesive states of cytoskeleton-coupled Ecads represent different Ecad conformations. Since we have previously shown that Ecad ectodomains can be trapped in an X-dimer conformation simply by incubating them in free Trp (8), we performed AFM measurements on parental-Trp cells to identify the signature of X-dimer formed by cytoskeleton-coupled Ecads. Interestingly, almost all (99% ± 13%) cytoskeleton-bound Ecads in parental-Trp formed jump events (Fig. 4*B*), suggesting that the jump events represent Ecads that form X-dimers. This, along with the exclusive presence of jumps in vinc-KO and ΔVBS (Fig. 4*B*), indicates that the weakening of Ecad adhesion in the absence of vinculin binding is consistent with Ecads being trapped in an X-dimer conformation. Importantly, switching ectodomains into an X-dimer conformation did not decouple Ecad from the cytoskeleton and the fraction of cytoskeleton-coupled Ecad in the Trp

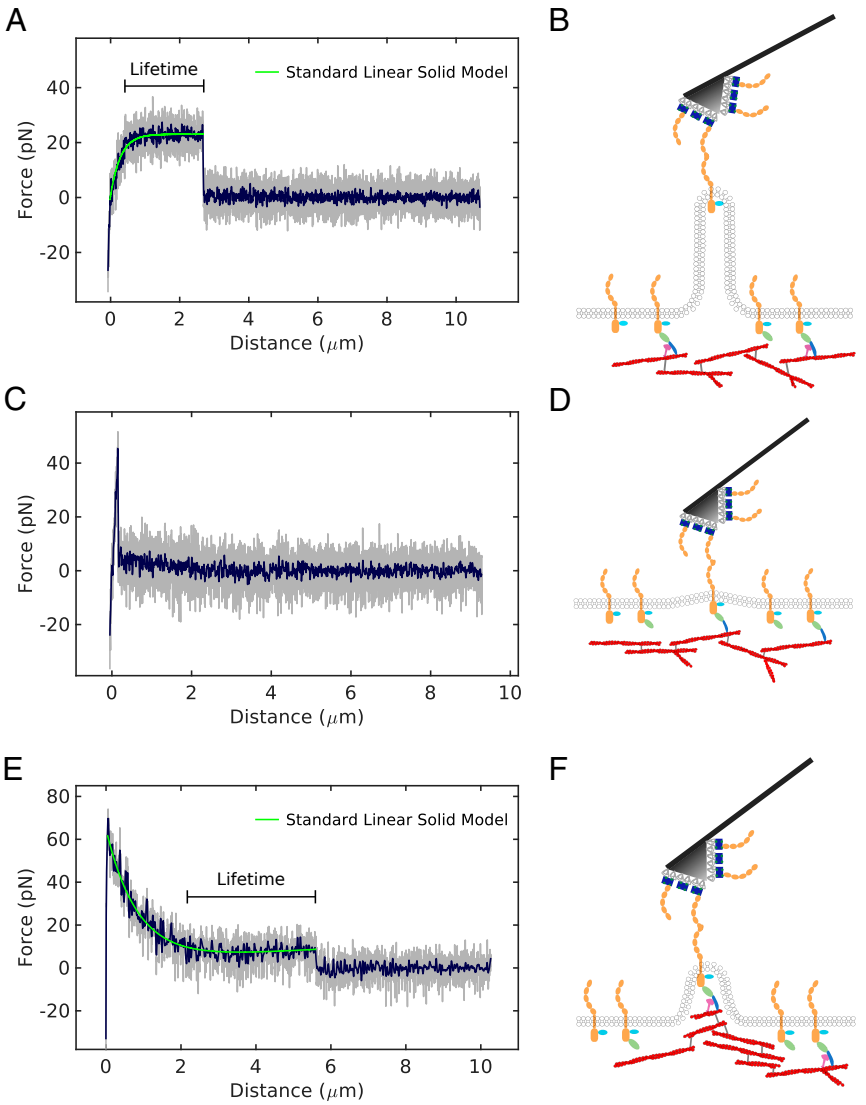


**Fig. 3.** Force "signatures" used to identify cytoskeletal coupling and strength of *trans* adhesion. (*A*) Typical force curve showing a membrane tether which extends at a constant force. (*B*) Membrane tethers are measured when an Ecad which is not linked to the actin cytoskeleton is pulled. (*C*) Jump events exhibit a linear increase in force and are measured upon pulling (*D*) an Ecad *trans* dimer that is weaker than its cytoskeleton coupling. (*E*) Typical force curve showing a cyto tether with an initial increase in force that viscoelastically relaxes as a membrane tether is formed. (*F*) Cyto tethers are measured when a robust Ecad *trans* dimer that is linked to the actin cytoskeleton is pulled. Raw data (gray) were acquired at 25 kHz and smoothed (blue) to 111 Hz. Green curve is the SLS model fit to membrane tethers and cyto tethers. Black bars indicate bond lifetimes determined from membrane tethers and cyto tethers.

treated cells (52% ± 5%) remained the same as parental cells (Fig. 4*A*).

We also inferred the *trans* dimer binding conformation of cytoskeleton-coupled Ecad in the parental-Trp, vinc-KO, and ΔVBS cells using dynamic force spectroscopy (DFS) analysis (37). Since the number of jump events in vinc-KO cells was insufficient to obtain statistically reliable results, we combined the vinc-KO jumps with the jumps measured with ΔVBS cells. The measured intrinsic off rate ($k_{off}$) for jump events for vinc-KO and ΔVBS ($k_{off}$ = 1.77 ± 0.51 $s^{-1}$; Fig. 4*C*) was comparable to parental-Trp X-dimers ($k_{off}$ = 1.73 ± 0.62 $s^{-1}$; Fig. 4*D*) and higher than previously published values for strand-swap dimers (38–41). Since a higher $k_{off}$ corresponds to a weaker binding, these data further suggest that in the absence of vinculin association, cytoskeleton-coupled Ecad adopts a weaker X-dimer conformation.

Next, since cadherins trapped in an X-dimer conformation have delayed junction formation (42), we monitored the formation of cell–cell barriers in parental-Trp and ΔVBS cells using electric cell-substrate impedance sensing (ECIS), in order to determine if the junction formation in these cell lines is consistent with Ecad's adopting an X-dimer conformation. Our experiments measuring the barrier formation half-time (T50) showed a significant delay in calcium-induced barrier formation in parental-Trp and ΔVBS cells compared to parental cells (parental-Trp 1.23 ± 0.65 h delay in T50, ΔVBS 3.66 ± 2.26 h delay in T50; Fig. 4*F*). Importantly, delayed barrier formation with ΔVBS was consistent with previous reports (26). Taken together, our ECIS results indicate that both Ecad conformation and vinculin binding to α-catenin are important for the formation of cadherin junctions and further suggest that vinculin is responsible for regulating Ecad conformation.

**Ecad Ectodomain Conformation Is Regulated by Vinculin.** Next, we proceeded to directly measure the binding conformation of Ecad ectodomains in the different cell lines by measuring if the Ecads

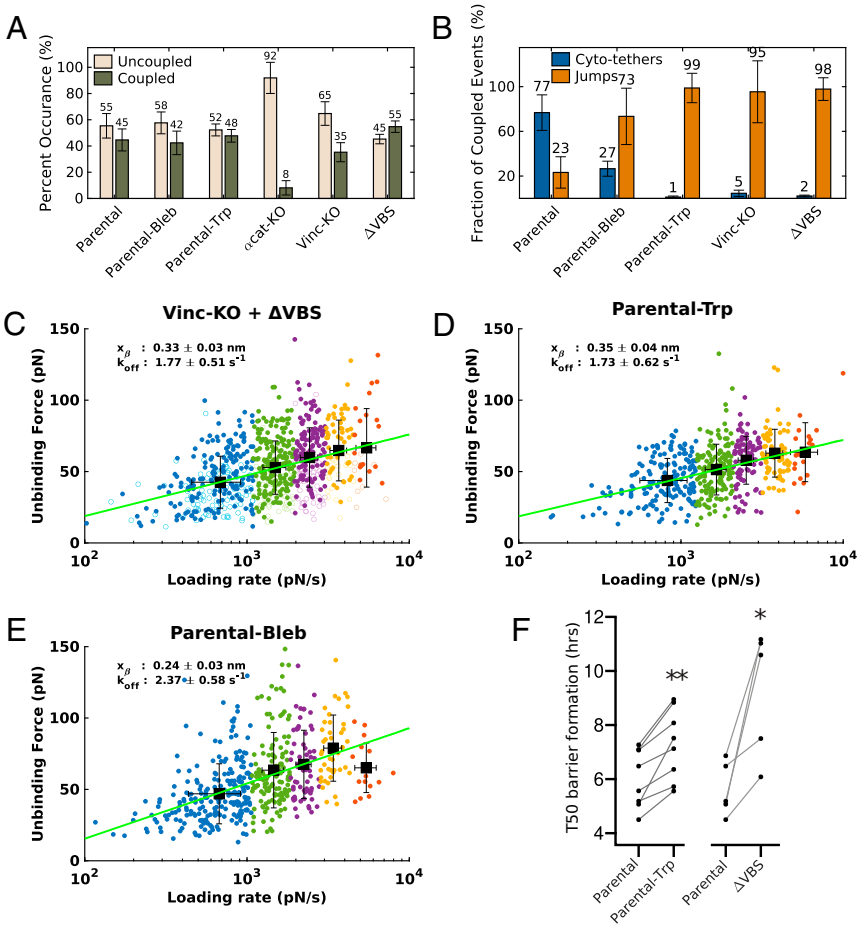


**Fig. 4.** Role of α-catenin and vinculin in Ecad-cytoskeleton linkage and adhesion strength. (*A*) Fraction of uncoupled (membrane-tether) and coupled (cyto-tether + jump) events. Fractions were calculated after subtracting the binding probability of the control experiment for each cell line. (*B*) Fractions of strong (cyto-tether) and weak (jump) Ecad *trans* dimer events. Error bars are the propagated errors obtained from bootstrapped SDs. DFS of jump events in (*C*) vinc-KO + ΔVBS, (*D*) parental-Trp, and (*E*) parental-Bleb cells. Loading rates and peak forces in jump events were bootstrapped 1,000 times then clustered using *k*-means and fit to the Bell–Evans model (green line) using weighted nonlinear least-square fitting. Data points represent single unbinding events, and colors correspond to data points from the same *k*-means cluster. The data from ΔVBS (filled circles) and vinc-KO (circles) cells in *C* were combined because the number of data points were insufficient for a statistically reliable calculation. Intrinsic off rate ($k_{off}$) and distance to the transition energy barrier ($x_\beta$) were obtained from the mean of the fitted parameters acquired by fitting the *k*-means clusters that were calculated from the bootstrapped samples. Errors in the fitted parameters correspond to SDs of the bootstrapped means. (*F*) Transepithelial resistance measurement of parental cells in the absence (Parental; $n = 9$) and presence (Parental-Trp; $n = 8$) of 2 mM tryptophan, or ΔVBS cells (ΔVBS; $n = 5$), following addition of 2 mM $CaCl_2$ to induce Ecad-dependent formation of the epithelial barrier. Barrier formation half-times (T50) were calculated as the time point at which the impedance signal surpassed 50% of the ultimate maximum impedance. $^*P = 0.0025$, $^{**}P = 0.0011$; paired *t* test.

on the cell surface form catch bonds (X-dimers) or slip bonds (strand-swap dimers). We measured the force vs. lifetimes of Ecad–Ecad bonds, using a method described previously (43). Briefly, since the force required to rupture membrane tethers and cyto tethers scales linearly with pulling velocity (28, 44) (*SI Appendix*, Fig. S2), and because these tethers extend at a constant force (after any initial viscoelastic relaxation) when pulled at a constant velocity (27, 31) (Fig. 3 *A* and *E*), we determined bond lifetimes at a range of forces from the persistence time of membrane tethers and cyto tethers.

We first measured the force vs. lifetime of Ecad endogenously expressed on the apical surface of parental cells. Fits of our data to the composite of a slip bond (45) and catch bond (46) model showed that 69% of Ecads in the parental cells form strand-swap dimers while the remaining 31% of Ecads occupy an X-dimer conformation (Fig. 5*A*, *Methods*, and *SI Appendix*, Table S2). Upon Trp incubation, however, Ecads in parental cells switched their conformation and formed catch bonds characteristic of an X-dimer (Fig. 5*B*).

Since the bond lifetimes for parental cells (Fig. 5*A*) were obtained from all the tethers (a mix of cyto tethers and membrane tethers), we separately analyzed the force-dependent lifetimes of cyto-tether and membrane-tether events (*SI Appendix*, Fig. S3 *A* and *B*). Consistent with cyto tethers corresponding to strong Ecad–Ecad bonds, our analysis showed that cyto tethers (which correspond to Ecad initially coupled to the cytoskeleton) exclusively formed slip bonds. Ecads that were decoupled from the cytoskeleton (membrane-tether events) formed X-dimers and strand-swap dimers with almost equal probabilities (45% catch bonds : 55% slip bonds) (*SI Appendix*, Fig. S3 *A* and *B*). This provided further evidence that the association of vinculin with the Ecad cytoplasmic domain is required for ectodomains to efficiently form strand-swap dimers.

As anticipated from our DFS experiments, Ecads in the vinc-KO cells formed catch bonds characteristic of an X-dimer conformation (Fig. 5*C*), suggesting that vinculin association is necessary for Ecads to form robust strand-swap dimers. Similarly, Ecads in αcat-KO cells, where vinculin cannot associate with the Ecad

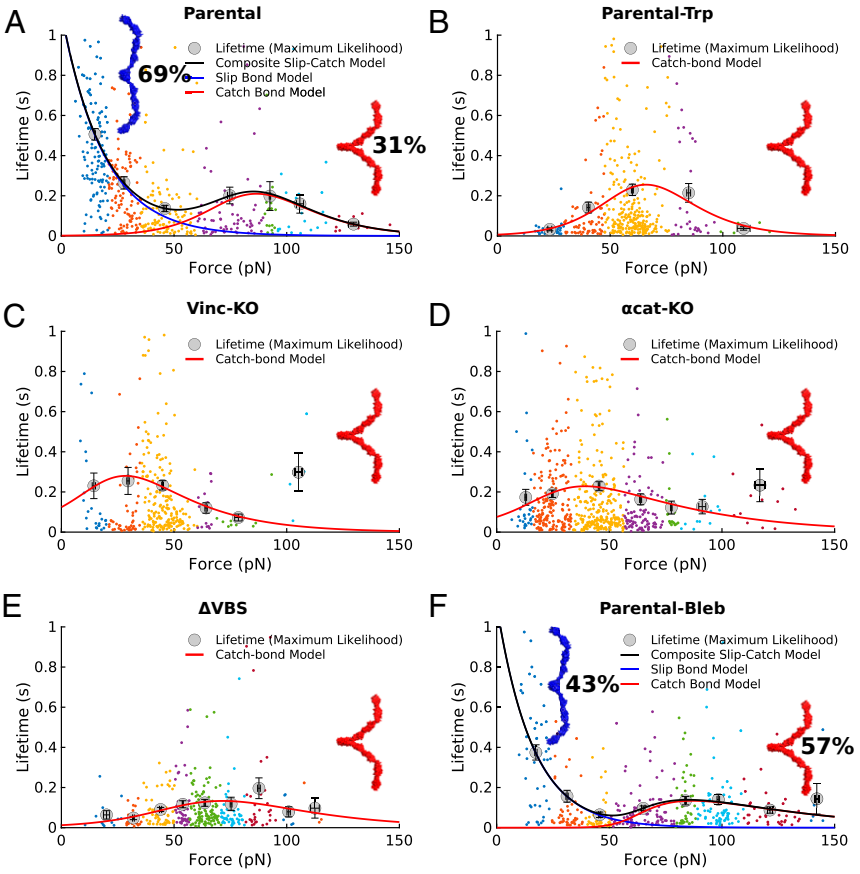


**Fig. 5.** Measuring conformation of Ecad *trans* dimers using an AFM. Force vs. lifetime profile for (*A*) parental cells shows that 69% of Ecad form slip bonds (strand-swap dimer structure shown in blue) and the remaining 31% form catch bonds (X-dimer structure shown in red). (*B*) Parental-Trp, (*C*) vinc-KO, (*D*) αcat-KO, and (*E*) ΔVBS cells form catch bonds. (*F*) Inhibition of myosin II using blebbistatin reduces the fraction of slip bond forming Ecad. Parental-Bleb shows that 43% of Ecads form slip bonds and the remaining 57% form catch bonds. Solid lines represent fits to the corresponding models. Data were binned using a Gaussian mixture model and the lifetimes were determined using maximum likelihood estimation. The colored data points correspond to the data points in each respective bin. The data were fit by $\chi^2$ minimization and errors were obtained by bootstrapping. The *y* axes were limited to 1 s for clarity.

cytoplasmic region (12), also formed catch bonds (Fig. 5*D*). Finally, eliminating vinculin binding to α-catenin in ΔVBS cells also resulted in catch bonds (Fig. 5*E*), confirming that association of vinculin with the Ecad cytoplasmic region via α-catenin is obligatory for transitioning from a weak X-dimer conformation to a robust strand-swap dimer conformation.

**Regulation of Ecad Ectodomain Conformation Is Myosin II Dependent.** Having identified vinculin as a key protein involved in allosterically regulating Ecad ectodomain conformation, we proceeded to identify the mechanism by which vinculin regulates Ecad structure. Since vinculin localizes to force-bearing sites in the cell–cell junction and mediates the recruitment of myosin II (18), we hypothesized that Ecad ectodomain conformation could be regulated by myosin II–mediated cytoskeletal contractile force. We therefore tested the effect of myosin II–mediated force on Ecad conformation in parental cells by reducing cytoskeleton contractility using the myosin II inhibitor blebbistatin (parental-Bleb). Strikingly, in parental-Bleb cells, the fraction of Ecad in strand-swap dimer conformation (43%; Fig. 5*F*) decreased compared to parental cells (69% strand-swap dimer; Fig. 5*A*). This indicated that myosin II–dependent cytoskeletal contractility plays a role in driving strand-swap dimerization of Ecad ectodomains.

Additionally, unlike parental cells where the majority of cytoskeleton-coupled Ecad existed in the robust binding conformation (cyto tethers), most of the cytosekeleton-coupled Ecad in parental-Bleb formed weak binding structures (jumps) (27% ± 7% cyto tethers and 73% ± 25% jumps; Fig. 4*B*). Importantly, the fraction of cytoskeleton-coupled Ecad in parental-Bleb (42% ± 9%; Fig. 4*A*) remained the same as in parental cells. Finally, the measured $k_{off}$ for jump events in parental-Bleb (2.37 ± 0.58 $s^{-1}$; Fig. 4*E*) was comparable to the values measured for X-dimers formed by parental-Trp, vinc-KO, and ΔVBS cells (Fig. 4 *C* and *D*). Taken together, these data confirm that reduced myosin II–dependent cytoskeletal contractility reduces the ability of Ecad to form robust strand-swap dimers.

Since forces generated by the actomyosin cytoskeleton can transmit to the Ecad cytoplasmic domain (47), we used steered molecular dynamics (SMD) simulations to test if force could convert X-dimers to strand-swap dimers (Fig. 6 *A* and *B*). We modeled cytoskeletal forces by pulling on the C terminus of the EC1-2 X-dimer crystal structure (Protein Data Bank [PDB] ID code 3LNH) at five angles (0°, ±30°, and ±40°), chosen to account for different orientations of actin filaments (Fig. 6*B*). Our simulations showed that regardless of the pulling angle all X-dimers converted to strand-swap dimers after a period of force application (Fig. 6 *B* and *C*). Rmsds of the SMD structures, calculated relative to the strand-swap dimer crystal structure (PDB ID code 2QVF), converged to an average of 0.67 ± 0.12 nm, confirming that the structures closely resembled strand-swap dimers (Fig. 6*C*). These simulations confirm that when Ecad dimers are firmly coupled to the actin cytoskeleton by α-catenin and vinculin, myosin II–dependent force can convert X-dimers to strand-swap dimers.

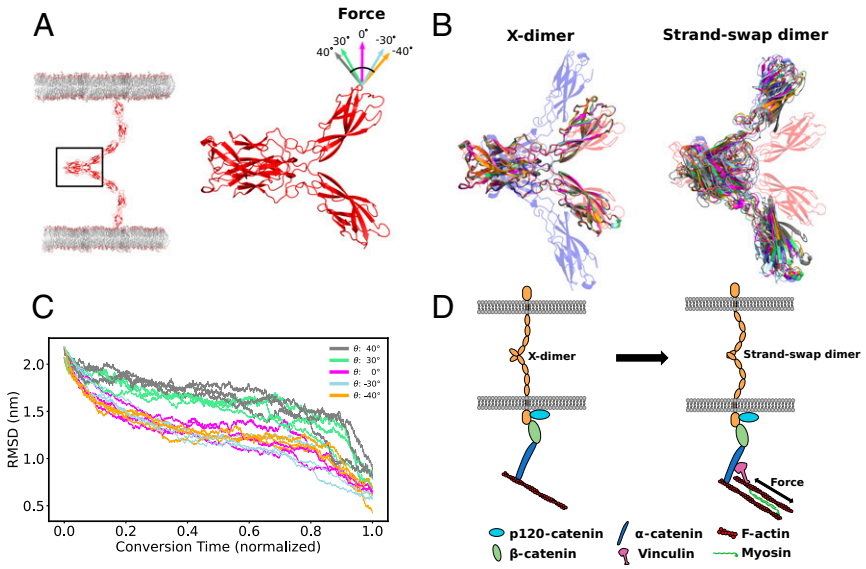


**Fig. 6.** Cytoskeletal tension converts X-dimers to strand-swap dimers. (*A*) X-dimer formed by Ecad on opposing cells (*Left*). X-dimer crystal structure (PDB ID code 3LNH) used in SMD simulations (*Right*). The pulling directions are indicated by colored arrows. The full X-dimer (*Left*) was modeled by aligning 3Q2V to 3LNH. (*B*) X-dimer conversion to strand-swap dimer. Simulated structures remain in an X-dimer conformation after stabilizing MD simulations (*Left*). X-dimers become strand-swap dimers after pulling on the C-terminal of one Ecad at a range of angles (*Right*). The transparent blue structure is the strand-swap crystal structure (PDB ID code 2QVF). The transparent red structure is the X-dimer crystal structure (PDB ID code 3LNH). The remaining, opaque structures are the simulated structures. (*C*) Rmsd of the pulled structures relative to the strand-swap dimer crystal structure as a function of the time it took to converge to the strand-swap crystal structure (minimum rmsd). Rmsds were determined by least-squares fitting to the strand-swap dimer crystal structure and calculating the distance between alpha carbons of the two structures. (*D*) Model for vinculin-dependent, force-induced conversion of X-dimers to strand-swap dimers. In the absence of vinculin, force applied is insufficient to convert the X-dimer to a strand-swap dimer (*Left*). Cytoskeletal tension is transmitted in a vinculin-dependent manner to the Ecad extracellular bond to promote conversion to a strand-swap dimer (*Right*).



## Discussion

Using live-cell, single-molecule AFM measurements we directly demonstrate inside-out regulation of cadherin conformation and show that cytoplasmic proteins regulate Ecad adhesive properties, similar to inside-out regulation of integrins (48). Our data establish a distinct, mechanistic role for vinculin in allosterically regulating Ecad conformation and adhesion at the single-molecule level. Our results also demonstrate that previous interpretations of how vinculin strengthens Ecad adhesion are incomplete. While previous studies solely focused on vinculin-mediated remodeling of the junctional actomyosin cytoskeleton (22–24), we demonstrate that vinculin also changes the adhesive properties of individual Ecad ectodomains. Furthermore, our data suggest that vinculin mediates the transmission of cytoskeletal contractile force to the Ecad ectodomain and drives the conversion of X-dimers to strand-swap dimers. Consequently, when Ecads decouple from vinculin and/or α-catenin, they are trapped in an X-dimer structure. Force-induced changes in Ecad dimer conformation has been previously suggested (7) but until now has not been directly measured.

While previous AFM measurements with α-catenin knockdown cells suggest that reducing α-catenin levels decrease the unbinding force of Ecad ectodomains, the molecular mechanism by which α-catenin influences Ecad adhesion was not determined (49, 50). Our data show that vinculin association and myosin II–dependent cytoskeletal contractility allosterically trigger strand-swap dimerization of Ecad and suggest that α-catenin affects Ecad adhesion by serving as the scaffold protein that binds vinculin to Ecad–catenin complex.

It is important to point out that our experiments measure the allosteric conformational regulation of nonjunctional Ecads present on the apical surface of cells. While apical Ecads may be organized differently from Ecads localized to cell–cell junctions (51, 52), the intracellular proteins that couple Ecad to the actin cytoskeleton are similar for both Ecad pools. Previous studies show that both apical and junctional Ecads are under similar levels of constitutive actomyosin tension (47), suggesting that both Ecad pools interact with the actin cytoskeleton in similar manners. Moreover, magnetic twisting cytometry shows force-induced, vinculin-dependent stiffening of Ecad-coated beads placed on the apical cell surface, suggesting that vinculin also associates with the extrajunctional Ecad (18). More recently, three-dimensional superresolution microscopy of MDCK cells attached to an Ecad-coated substrate show that the intracellular organization of many Ecad-associating proteins including p-120 catenin, β-catenin, α-catenin, and vinculin resemble native cell–cell junctions (53). These studies suggest that the inside-out regulation that we measure with apical Ecads also occurs with junctional Ecads.

Our ECIS experiments show that while barrier formation half-time for both parental-Trp and ΔVBS cells was longer compared to parental cells (Fig. 4*F*), the maximum impedances after barrier formation was completed for parental and ΔVBS cells were similar to each other and slightly higher than parental-Trp cells (*SI Appendix*, Fig. S4). This finding is explained by the fact that the maximum impedance is a measure of the steady state of barrier integrity after the dynamic process of junction formation is completed and is principally determined by formation of tight junctions. Consequently, given enough time, the clustering of Ecads within ΔVBS junctions could orient them to promote formation of strand-swap dimers, similar to parental cells. However, when Trp is added to the parental cells it blocks strand-swapping and traps Ecad in an X-dimer conformation even when junction formation is completed and reaches steady state. Previous studies show that tight junctions in Ecad-deficient mice have increased permeability (54). This suggests that inhibiting strand swapping in Ecad may affect tight junction formation, resulting in a lower maximum impedance in parental-Trp cells.

Despite the large number of proteins expressed on the cell surface, we were able to measure single-molecule unbinding by

limiting Ecad density on the AFM tip and controlling the force with which the AFM tip contacts the cell. However, we were also aided by a low density of Ecads expressed on the apical surface of confluent MDCK cell monolayers. While the precise oligomeric state of Ecad on apical cell surfaces is unclear, with superresolution imaging suggesting that apical Ecads in A431 cells are present as well separated monomers (51) while Ecads in A431D cells organize into small nanoclusters (52), our low unbinding event rates nonetheless suggest that only single Ecads on the AFM tip interact with Ecads on the cell surface, even if a direct comparison between MDCK and A431/A431D cells cannot be made, potentially due to their different properties. Interestingly, the total Ecad event rate measured with αcat-KO cells is higher than with parental, ΔVBS, or vinc-KO cells (Fig. 2*B*). This likely occurs because the αcat-KO cells do not form stable cell–cell junctions (25). Consequently, Ecads that would otherwise be corralled within cell–cell junctions are now redistributed on the apical cells surface and subsequently interact with Ecads on the AFM tip with a higher probability. The same may be true for other membrane proteins, which contributes to an increase in nonspecific event rate in control experiments with αcat-KO cells (Fig. 2*B*).

Although AFM is uniquely suited to study the biomechanics of membrane proteins, as with any experiment there are limitations. The cell surface is a complex environment with many molecules and it is difficult to determine which cell-surface protein is interacting with Ecad on the AFM tip. For this reason, we engineered the Ecad-KO cell lines and show that we are not observing any significant heterophilic interactions. For instance, while Ecad can interact heterophilically with several transmembrane proteins, including Desmoglein-2 (Dsg2) and P-cadherin (Pcad) (55, 56), our control measurements with Ecad-KO cells show that there is no significant binding of Ecad with other cell-surface proteins (Fig. 2*B*). The binding rates measured for the interaction between an AFM tip functionalized with Ecad and the Ecad-KO cells (which corresponds to heterophilic binding between Ecad on the AFM tip and other proteins expressed in MDCK cells) is similar to the binding rate for a bare AFM tip lacking Ecad and parental MDCK cells expressing all transmembrane proteins. This demonstrates that heterophilic Ecad interactions on the apical cell surface occur at such a low rate that we are unable to detect them. One possible reason for the low heterophilic binding of Ecad is that other transmembrane binding partners may have low expression on the apical surface of MDCK cells. We tested this by comparing the fraction of apically expressed Ecad and Pcad using nonjunctional protein biotinylation in MDCK cells (57, 58). Quantitative analysis demonstrated that the fraction of nonjunctional Ecad was at least an order of magnitude greater than the Pcad fraction located outside cell–cell junctions (*SI Appendix*, Fig. S5).

In addition to low apical surface expression level, the affinity of Ecad heterophilic binding may be lower compared to Ecad–Ecad interactions, resulting in low heterophilic interactions. Furthermore, since the structures of Ecad bound to different heterophilic binding partners are unknown, our experimental design may also preclude some of these interactions from occurring. For instance, since Dsg2 binds to the *cis* interface of Ecad (55), this would require tethered Ecads on the AFM cantilever to flip their orientation and interact with Dsg2 on the cell surface, an event that has a low probability of occurring. However, we cannot completely eliminate the possibility of some heterophilic binding in our experiments as it is possible that the knock-out cells have different localization of other Ecad binding partners. It is also important to note that since our cells are grown on nonporous glass coverslips for up to 72 h, they are, at best, only partially polarized. Consequently, while some microvilli or primary cilia may be present on the apical cell surface, the probability of probing Ecad on these structures is quite low.

Previous studies also suggest that α-catenin is not the sole linker of Ecad and the cortical actin cytoskeleton. The binding of β-catenin to vinculin is believed to serve as an alternate, secondary bypass connection between Ecad and F-actin (59). However, this alternate coupling is believed to be initiated by α-catenin (60). Our AFM data are consistent with these findings. The fraction of cytoskeletal-linked Ecad in both parental and ΔVBS cells, which presumably contain the primary α-catenin/F-actin and the secondary β-catenin/vinculin linkages, is similar (Fig. 4*A*). In contrast, in vinc-KO cells, which presumably contain α-catenin/actin linkages but do not contain β-catenin/vinculin linkages, we see a reduced coupling of Ecad to the actin cytoskeleton (Fig. 4*A*). Finally, in αcat-KO cells we see practically no coupling between Ecad and F-actin, presumably because both the primary α-catenin/actin and the alternate β-catenin/vinculin linkages cannot be formed (Fig. 4*A*). However, our data do not eliminate the possibility that the greater fraction of Ecad–actin linkages in ΔVBS cells compared to vinc-KO cells occurs because the ΔVBS cells contain higher amounts of cytoplasmic α-catenin (Fig. 1*C*).

It is also worth noting that measurements in αcat-KO cells—where Ecad cannot link to actin cytoskeleton—mainly resulted in membrane tethers (Fig. 4*A*), validating the use of membrane tethers as a signature of cytoskeleton-uncoupled Ecad. Furthermore, the very low occurrence of jumps and cyto tethers in αcat-KO cells (Fig. 4*A*) implies that jumps and cyto tethers indeed correspond to the pulling of Ecad coupled to the underlying cytoskeleton. Additionally, the presence of only jumps in the parental-Trp, vinc-KO, and ΔVBS cells (Fig. 4*B*), where Ecad exclusively formed weaker X-dimers (Fig. 5 *B*, *C*, and *E*), supports that jumps represent X-dimers linked to the actin cytoskeleton. Finally, the decrease in fraction of cyto tethers (Fig. 4*B*) with the decreased probability of strand-swap dimer formation in parental-Bleb (Fig. 5*F*) strongly suggests that cyto tethers correspond to strand-swap dimers linked to the actin cytoskeleton. While Ecads in parental cells that are coupled to the cytoskeleton via α-catenin and vinculin (cyto-tethers) exclusively formed strand-swap dimers, we were surprised to observe that Ecads which are decoupled from the cytoskeleton (membrane tethers) formed X-dimers and strand-swap dimers with coequal probabilities (*SI Appendix*, Fig. S3 *A* and *B*). A likely explanation for this result is that the Ecad–cytoskeletal linkage is dynamic and that even transient interactions with vinculin are sufficient to drive strand-swap dimer formation. Since the AFM tip and the cell surface remain in contact for about 0.45 s in our experiments (*SI Appendix*, Fig. S6), this may allow enough time for Ecads on the parental cells to convert to a strand-swap dimer conformation and detach from the cytoskeleton (thereby forming membrane tethers), before the AFM tip is withdrawn from the cell surface.

When parental cells were treated with blebbistatin, the reduced actomyosin tension resulted in a decrease in the fraction of cyto tethers (Fig. 4*B*). While these cyto tethers behaved like parental cyto tethers and exclusively formed slip bonds (*SI Appendix*, Fig. S3*C*), a larger fraction of parental-Bleb membrane tethers formed X-dimers compared to parental cells (69% in parental-Bleb compared to 55% in parental cells), further demonstrating that myosin-generated contractile force is important for cadherin strand-swap dimer formation (*SI Appendix*, Fig. S3*D*).

Given the higher lifetimes for X-dimers compared to strand-swap dimers at forces >50 pN (Fig. 5*A*), it might be expected that force would convert Ecad to X-dimers instead of strand-swap dimers. However, since contractile force applied by actomyosin on a single Ecad is only around 1 to 2 pN (47) and the lifetime of the strand swap dimer is higher than the X-dimer at forces <~50 pN, (Fig. 5*A*), the strand-swap dimer is the preferred binding conformation in a physiological context. Furthermore, as shown

by our simulations (Fig. 6 *A* and *C*), the geometry of these conformations does not permit a transition from strand-swap dimer to X-dimer since pulling on the strand-swap dimer moves the X-dimer interface further apart.

Consistent with a previous study that used optical tweezers and single-particle tracking to infer the fraction of cytoskeleton-bound Ecad (36), our data show that only ∼50% of Ecads on the apical cell surface are coupled to the actin cytoskeleton. Studies also show that cells expressing Ecad/α-catenin fusion constructs that constitutively bind to the actin cytoskeleton exhibit higher cell–cell adhesion and reduced intercellular motility compared to cells expressing wild-type Ecad (36, 61). These findings are supported by our observation that two rapidly exchangeable pools of Ecad structures (X-dimers and strand-swap dimers) exist on the cell surface. It is likely that these different pools of Ecads are crucial in reorganizing cell–cell junctions during collective cell migration: As the cell–cell contacts rapidly rearrange, strand-swap dimers anchor the contact while X-dimers probe for formation of new contacts.

Based on the results presented in this paper, we propose a biophysical model for the inside-out regulation of Ecad conformation. Our data suggest that vinculin-mediated myosin II recruitment generates a contractile force which propagates to the Ecad ectodomain and drives the conversion of X-dimers to strand-swap dimers (Fig. 6*D*). Consequently, treating parental cells with blebbistatin, inhibits myosin II–dependent cytoskeletal contractility and reduces the ability of Ecad to form robust strand-swap dimers (Fig. 5*F*). All atom computer simulations also demonstrate that a force applied to the membrane proximal region of X-dimers results in formation of strand-swap dimers (Fig. 6 *B* and *C*). Previous studies suggest that Ecad adhesion is altered by changing the phosphorylation state of cytoplasmic p120-catenin (40, 62, 63); however, the mechanism by which this occurs and the exact conformational states Ecads adopt are unknown. It is possible that p120-catenin also indirectly modulates vinculin association with the Ecad cytoplasmic region, which in turn regulates Ecad ectodomain conformation and adhesion.

Recent studies have suggested that regulation of Ecad adhesion plays an important role in cancer progression. For instance, it has been shown that up-regulation of Ecad adhesive activity, rather than its amount, reduces the number of cells metastasized from the mammary gland to the lung (64). Additionally, several point mutations in Ecad ectodomains that are prevalent in hereditary diffuse gastric carcinoma selectively interfere with the inside-out regulation of Ecad adhesion, rather than the ability of Ecad to adhere (64). Furthermore, studies have shown that while vinculin expression is significantly reduced in colorectal cancer (CRC), overexpressing vinculin reduces metastasis in CRC (65) and other cancer cell lines (66). Consequently, understanding how cytoplasmic proteins induce conformational changes of Ecad ectodomains could be crucial to understanding the role of Ecad in cancer progression and metastasis.

## Methods

**Generating Mutant Cell Lines.** Generation of αcat-KO cells (ΔαE-catenin MDCK cells) (25) has been described previously. For generation of ΔVBS cells, αcat-KO cells were stably rescued (26) with GFP-α-catenin–ΔVBS mutants (35) as described previously. Vinc-KO and Ecad-KO cells were generated by stably expressing a PiggyBac plasmid encoding Cas9 with a cumate-inducible promoter and guide RNA (gRNA) expression cassette for canine Ecad or vinculin-specific gRNA, which resulted in complete knockout cells (see Fig. 1*C*). The mutations were sequence-verified by PCR amplifying the target sequences from genomic DNA of knockout cell lines and inserted into TOPO vectors (Invitrogen) for sequencing.

***Ecad:***

gRNA: ACAGACCAGTAACTAACGA

KO: ACAGACCAGT—AACGA

***Vinculin:***

gRNA: GGA GCACCGAGTAATGTTGG

KO: GGAtGCACCGAGTgATGTTGG

**Western Blotting.** Cell lysates for Western blotting were prepared in 1× sodium dodecyl sulfate (SDS) sample buffer (10 mM Tris, pH 6.8, 1% SDS, 10% glycerol, 0.005% bromophenol blue, and 2% β-mercaptoethanol). Primary antibodies against Ecad (clone 36; BD Biosciences), α-catenin (clone 15D9; Enzo Life Sciences), vinculin (clone hVIN-1; Millipore Sigma), and α-tubulin (clone DM1A; Cell Signaling) were used in manufacturer-recommended dilutions in phosphate-buffered saline with 0.1% Tween 20 (PBST). Horseradish peroxidase–conjugated secondary antibody (1706516; Bio-Rad) was used in 1:1,000 dilution in PBST. Protein samples were detected with a WesternBright Chemiluminescence Kit (K-12045; Advansta). Images were acquired using Image Lab software from Bio-Rad.

**Apical Surface Biotinylation.** Biotinylation of apical surface proteins was performed using a method described previously (58). Briefly, confluent monolayers of cells were washed with biotinylation buffer (10 mM Hepes, 130 mM NaCl, 2 mM $MgSO_4$, 1 mM $CaCl_2$, and 5.5 mM glucose, pH 7.9) at 4 °C and kept on ice for the rest of the biotinylation procedure. Apical cell surface proteins were biotinylated by a 15-min incubation with Sulfo-NHS-SS-Biotin (Thermo Fisher) at 1 mg/mL concentration. Excess Sulfo-NHS-SS-Biotin was removed and the reaction was quenched by washing two times with 100 mM glycine followed by 15-min incubation in the same buffer. Cells were lysed with a pH 7.5 buffer containing 150 mM NaCl, 50 mM Hepes, 5 mM ethylenediaminetetraacetic acid, 1% Triton X-100, 0.1% SDS, and protease inhibitor. Lysates were incubated with neutravidin-coated agarose beads (Thermo Fisher) overnight at 4 °C in chromatography columns to separate biotinylated proteins. Bead-unbound lysates were collected and the beads were washed with high-salt (1 M NaCl, 50 mM Hepes, and 0.1% Triton X-100, pH 7.4) buffer followed by no-salt (50 mM Hepes, pH 7.4) buffer. Biotinylated proteins were eluted by 20-min incubations at room temperature in pH 7.4 buffer containing 5% SDS, 100 mM NaCl, 100 mM dithiothreitol, and 5% β-mercaptoethanol and collected in two fractions of 200 μL each. Proteins were detected by Western blotting as described above using the following antibodies: Anti-Ecad (clone 36, 1:1,000 dilution; BD Biosciences), Anti-Pcad (clone 6A9, 1:500 dilution; Abcam), and anti–α-tubulin (clone DM1A, 1:1,000 dilution; Cell Signaling).

**Purification of Ecad Ectodomain.** Generation of Ecad monomer plasmids containing a C-terminal Avi tag has been described previously (67). The plasmids were incorporated into pcDNA3.1(+) vectors and were transiently transfected into HEK 293T cells using PEI (Milipore Sigma) as previously described (68). Three days posttransfection, conditioned media was collected for protein purification. Purification of Ecad were performed using methods described previously (8, 67). Media containing his-tagged Ecads was passed through a chromatography column containing Ni-NTA agarose beads (Qiagen). Beads were then washed with a pH 7.5 biotinylation buffer (25 mM Hepes, 5 mM NaCl, and 1 mM $CaCl_2$). Ecads bound to the Ni-NTA beads were biotinylated with BirA enzyme (BirA 500 kit; Avidity) for 1 h at 30 °C. Following biotinylation, free biotins were removed using the Ni-NTA column and biotinylated Ecads bound to Ni-NTA beads were eluted using a pH 7.5 buffer containing 200 mM Imidazole, 20 mM $Na_2HPO_4$, 500 mM NaCl, and 1 mM $CaCl_2$.

**Epithelial Barrier Formation Measurements.** Ecad-dependent formation of epithelial barriers was assessed by real-time impedance sensing. To this end, parental or ΔVBS cells were trypsinized, resuspended in calcium-free DMEM (D9800-10; Immunosource) supplemented with 10% dialyzed fetal calf serum, and plated onto L-cysteine–reduced, collagen I–coated 8WE10 electrodes (Applied Biophysics) at a density of $2 \times 10^5$ cells per well and in the presence or absence of 2 mM Trp. Impedance measurements were performed at 37 °C and 6% $CO_2$ using a 1600R ECIS system (Applied Biophysics) at a frequency of 4,000 Hz. $CaCl_2$ was added at a final concentration of 2 mM to allow for adherens junction formation, and measurements were continued until stable impedance levels were reached in all conditions. Within each individual experiment, four technical replicates for each condition were averaged to assess the time-dependent impedance for that condition. The half-times of barrier formation were calculated as the time point at which the impedance signal surpassed 50% of the ultimate maximum impedance.

**Ecad Functionalization on AFM Cantilever.** Purified Ecad monomers were immobilized on Si tip of AFM cantilevers (Hydra 2R-100N; AppNano) as described previously (8, 9, 55, 67). Briefly, the AFM cantilevers were cleaned by immersing in 25% $H_2O_2$/ 75% $H_2SO_4$ solution overnight. The cantilevers were then sequentially washed with deionized water and acetone. The cantilevers were functionalized with amine groups by immersing in 2% (vol/vol) 3-aminopropyltriethoxysilane

(Millipore Sigma) solution dissolved in acetone. Polyethylene glycol (PEG) (MW 5000; Lysan Bio) spacers containing amine-reactive *N*-hydroxysuccinimide ester group at one end were covalently attached to the cantilever (100 mg/mL in 100 mM $NaHCO_3$ dissolved in 600 mM $K_2SO_4$, for 4 h); 20% of the PEG spacers presented biotin molecules at the other end. Unreacted amine groups on the silane molecules were capped using NHS-sulfo acetate (10 mg/mL for 30 min; Thermo Fisher). PEG-functionalized AFM cantilevers were incubated in 1 mg/mL bovine serum albumin (55) overnight. The cantilevers were then sequentially incubated with streptavidin (0.1 mg/mL for 30 min) and biotinylated Ecads (200 nM for 90 min). Finally, free biotin-binding sites of streptavidin were blocked by using 0.02 mg/mL free biotin for 20 min. All steps, except the incubation with Ecad, were kept the same for cantilever functionalization in control experiments.

**Cell Culture for AFM Experiment.** Cells were cultured in low-glucose Dulbecco's modified Eagle's medium (DMEM) (Milipore Sigma) supplemented with 10% fetal bovine serum (Milipore Sigma) and 1% antibiotics solution (penicillin + streptomycin + kanamycin) at 37 °C and 5% $CO_2$. Cells were trypsinized 48 to 72 h prior to the experiment and plated on an ethanol-cleaned glass coverslip at a low density. The confluent monolayer of cells was washed five times with a pH 7 DMEM and antibiotics solution before loading onto the AFM setup with the same medium.

**AFM.** Force measurements were performed using two Agilent 5500 AFMs with closed loop scanners. An AFM cantilever functionalized with purified Ecad was brought in contact with a confluent monolayer of cells, pressed against the cell surface with a low force (typical pressing force was about 50 pN) for 0.1 s, and then retracted at one of five constant velocities (3, 5, 7, 9, or 11 μm/s). Control experiments used cantilevers decorated with streptavidin but lacking Ecad. Cantilever spring constants were measured using the thermal fluctuation method (69). All the experiments were performed in pH 7 DMEM and antibiotics solution in a custom-built environmental chamber supplied with 5% $CO_2$ at room temperature. Parental-Bleb and parental-Trp experiments were performed with 100 μM (±) blebbistatin (Milipore Sigma) and 2 mM L-tryptophan (Alfa Aesar) in the solution, respectively. A typical experiment lasted for ∼10 h, yielding ∼1,200 force–distance traces.

**Analysis of AFM Data.** AFM-generated force-distance traces were analyzed using custom MATLAB scripts. Traces containing single rupture events were classified into membrane-tether, jump, and cyto-tether categories based on the following criteria:

- Membrane tethers: force plateau at least 100 nm long and slope less than 25 pN/μm.
- Cyto tethers: have a difference between the peak force and the plateau force that is greater than the noise, calculated as 2 SDs of 500 data points after the force drop.
- Jumps: have a linear force–distance relationship with a slope of more than 25 pN/μm.

Rupture events having unbinding force less than the noise of each respective force curve or a force >150 pN were not considered for analysis. Tethers were further fit to the SLS model as described in (31) while jumps were fit to a Hookean spring model. We only retained events that fit either the SLS or spring model with a root-mean-squared error (RMSE) of less than the mean plus two SDs of all fits for each respective model.

To obtain the fractions of membrane-tether, cyto-tether, and jump events for each cell line we first measured the binding probability of each type of event for both the Ecad experiment and the control. The binding probabilities obtained from the control experiment were subtracted from the corresponding event rate of the Ecad experiment.

Loading rates for the jump events used for DFS analysis (Fig. 4 *C*–*E*) were calculated by multiplying the slope of the jump by the pulling velocity. *k*-means clustering was used to group the loading rates as described previously (70). Mean unbinding force and mean loading rate for the groups were fit using a weighted nonlinear least square fit to the Bell–Evans model (37). Raw data were bootstrapped with replacement, grouped using *k*-means, and the mean values were fit to the Bell–Evans model 1,000 times; the fitting parameters and errors were determined from the mean and SDs of the resulting distributions. The data used in each fit were weighted by the fraction of data points in a particular bin relative to the total number of data points. Force-dependent Ecad–Ecad bond mechanics were studied by analyzing the forces and lifetimes of membrane tethers and cyto tethers. Bond lifetimes were determined from the force curves starting at the beginning of the plateau region to the bond rupture. The unbinding force was calculated as the mean of the force values spanning that same region. These data were used to create the plots shown in Fig. 5. The unbinding forces were fit to a Gaussian mixture model (GMM) using an expectation maximization algorithm to determine the bins; the means and SDs used in the GMM fit were initialized using the *k*-means clustering algorithm. We determined the characteristic lifetime of each bin using maximum likelihood estimation (MLE) on bootstrapped samples. The likelihood function, $\mathcal{L}(\theta; X) = \prod_{i=1}^{N} f_i(x_i; \theta)$, was formulated using an exponential distribution *f*, where

$$f(x;\lambda) = \begin{cases} \lambda e^{-\lambda x} & x \geq 0, \\ 0 & x < 0. \end{cases}$$

The MLE lifetimes were fit by $\chi^2$ minimization to one of two models: a composite slip-catch bond model or a catch bond model (46). Assuming the errors in the measurements are Gaussian distributed, fitting by minimizing $\chi^2$ is the same as maximizing the log likelihood (46). The composite slip-catch model used to fit the parental and parental-Bleb data were the sum of a slip bond model and a catch bond model. The slip bond model (45), $\tau(F) = \frac{1}{k_{off}(F)} = \tau(0)e^{-\frac{Fx_\beta}{k_BT}}$, was used as the first component of the composite slip-catch model to fit the parental and parental-Bleb data (Fig. 5 *A* and *F*), where $\tau$ is the characteristic bond lifetime in the absence of force and $x_\beta$ is the reaction coordinate distance. The catch bond model used in the composite model and to fit all other cell lines is given by

$$\tau(F) = \frac{\sqrt{\pi} r_0 (E_1 - 2F(d + r_0)) e^{\beta(E_0 + dF)} \left(e^{\beta F r_0} - 1\right)}{4D(\beta E_0)^{\frac{3}{2}} F \left(1 + \frac{r_0}{d}\right)^2 \left(1 - e^{\beta(2F(d+r_0) - E_1)}\right)},$$

where $r_0$ is the natural bond length, $d$ is the reaction coordinate (same as $x_\beta$ for the slip bond model), $E_0$ and $E_1$ are components of the bond energy, $\beta = \frac{1}{k_BT}$ ($k_B$ is the Boltzmann constant), and $D$ is a diffusion constant ($D = \frac{k_BT}{6\pi\eta r_0}$). The number of bins used was established by the minimum weighted RMSE of the composite slip-catch or catch bond model relative to the MLE lifetimes when fitting the forces with the GMM using 5 to 10 bins (7 to 10 for parental and parental-Bleb) for each cell line. The weights were determined by the fraction of data points in a bin relative to the total number of data points for that cell line. The composite slip-catch and catch bond model fitted parameters are shown in *SI Appendix*, Table S2. The $\chi^2$ fitting function was acquired from the MathWorks File Exchange website (Generalized Nonlinear Nonanalytic Chi-Square Fitting by Nathaniel Brahms, 26 May 2006).

The fraction of strand-swap and X-dimers calculated from Fig. 5 *A* and *F* were determined by integrating each component of the composite model in 5-pN bins from 0 to 150 pN to determine the slip/catch area of that bin. The number of data points in each bin that corresponded to the slip bond model, for example, was determined by

$$\Delta n_{slip} = \left(\frac{\Delta A_{slip}}{\Delta A_{slip} + \Delta A_{catch}}\right) \Delta n,$$

where $\Delta A_{slip}$ and $\Delta A_{catch}$ are the area under slip and catch bond fit, respectively, for the 5-pN bin and $\Delta n$ is the total number of data points in the 5-pN bin. As expected, the sum of the slip and catch bond fits—and therefore the sum of their areas—is equal to the composite fit. The total fraction of data corresponding to the slip bond (strand-swap dimers) is then

$$Fraction_{slip} = \frac{\sum \Delta n_{slip}}{\sum \Delta n}.$$

**SMD Simulations and Structural Analysis.** SMD simulations were performed with GROMACS 2020.1 using the FARM high-performance computing cluster at University of California, Davis. The X-dimer crystal structure (PDB ID code 3LNH) was used in all simulations. Missing residues were added using PDBFixer and the N-terminal β-strand with Trp2 was positioned near the strand-swap interface using the sculpting tool in PyMOL. All simulations were performed with the OPLS-AA/L force field and the TIP4P water model.

The X-dimer crystal structure was equilibrated by performing a 20-ns molecular dynamics (MD) simulation. To setup the simulation, the X-dimer was placed in the center of a dodecahedral box such that no atom of the X-dimer was closer than 1 nm to any boundary. The box was solvated by adding water molecules and charge-neutralized by adding $Na^+$ ions. Additionally, NaCl, KCl, and $CaCl_2$ were added to the box at concentrations of 150 mM, 4 mM, and 2 mM, respectively, for a total system size of 148,965 atoms. Energy minimization, using the steepest decent algorithm, was performed until the force on any atom in the system was less than 1,000 $kJ{\cdot}mol^{-1}{\cdot}nm^{-1}$. The temperature, pressure, and density of the system were stabilized by equilibrating under isothermal–isochoric and isothermal–isobaric conditions

using a modified Berendsen thermostat and Berendsen barostat. Following equilibration, a 20-ns MD simulation was performed with 2-fs integration steps and LINCS constraints on bond length, and long-range interactions were evaluated using the particle mesh Ewald method. The stability of the X-dimer was monitored by calculating the rmsd of the X-dimer relative to the initial structure.

Conformational switching was modeled using SMD simulations performed on the fully equilibrated X-dimer by pulling on a group of residues (residues 151 to 166, 174 to 186, and 208 to 213)—to avoid unfolding—at the C-terminal end of one Ecad monomer in five directions (0°, ±30°, and ±40°; see Fig. 6*A*). The C-terminal of the opposing Ecad was constrained to simulate a robust linkage to the actin cytoskeleton. The X-dimer structure from the final frame of the MD simulation was placed at the center of a 12- × 30- × 8-nm$^3$ box and solvated and equilibrated as described above to an average of 376,743 atoms. After centering the X-dimer in the box, the pulling angle was achieved by rotating the X-dimer about the *z* axis (short axis) by the corresponding pulling angle. For each simulation, the X-dimer was pulled with a constant force (force constant = 498.2 pN/nm; 300 kJ·mol$^{-1}$·nm$^{-2}$) along the long axis of the box.

The conversion of the X-dimer to strand-swap dimer was determined by aligning the simulated structures to the X-dimer (PDB ID code 3LNH) and strand-swap dimer (PDB ID code 2QVF) crystal structures and calculating the rmsd of the alpha carbon atoms before and after pulling, respectively. The strand-swap dimer was formed from 2QVF by crystallographic symmetry operations.

**Data Availability.** All study data are included in the article and/or *SI Appendix*.

**ACKNOWLEDGMENTS.** Research in the S.S. laboratory was supported in part by the NSF (grant PHY-1607550) and the National Institute of General Medical Sciences of the NIH (grants R01GM121885 and R01GM133880). Research in the S.Y. laboratory was supported by the NIH (grant R03EB021636), the NSF (grant 1562095, Research Experiences for Undergraduates supplement to J.S.C.), and a University of California, Davis Provost's Undergraduate Fellowship (to J.S.C.). J.S.C. is a recipient of the Beckman Scholars Award. Research in the M.G. laboratory was supported by the Netherlands Organization for Scientific Research (grants NWO 016.Vidi.189.166 and NWO gravitational program 024.001.028).

1. A. M. Mendonsa, T.-Y. Na, B. M. Gumbiner, E-cadherin in contact inhibition and cancer. *Oncogene* **37**, 4769–4780 (2018).
2. T. J. Boggon *et al*., C-cadherin ectodomain structure and implications for cell adhesion mechanisms. *Science* **296**, 1308–1313 (2002).
3. D. Häussinger *et al*., Proteolytic E-cadherin activation followed by solution NMR and X-ray crystallography. *EMBO J.* **23**, 1699–1708 (2004).
4. E. Parisini, J. M. G. Higgins, J. H. Liu, M. B. Brenner, J. H. Wang, The crystal structure of human E-cadherin domains 1 and 2, and comparison with other cadherins in the context of adhesion mechanism. *J. Mol. Biol.* **373**, 401–411 (2007).
5. S. Sivasankar, Y. Zhang, W. J. Nelson, S. Chu, Characterizing the initial encounter complex in cadherin adhesion. *Structure* **17**, 1075–1081 (2009).
6. O. J. Harrison *et al*., Two-step adhesive binding by classical cadherins. *Nat. Struct. Mol. Biol.* **17**, 348–357 (2010).
7. S. Hong, R. B. Troyanovsky, S. M. Troyanovsky, Cadherin exits the junction by switching its adhesive bond. *J. Cell Biol.* **192**, 1073–1083 (2011).
8. S. Rakshit, Y. Zhang, K. Manibog, O. Shafraz, S. Sivasankar, Ideal, catch, and slip bonds in cadherin adhesion. *Proc. Natl. Acad. Sci. U.S.A.* **109**, 18815–18820 (2012).
9. K. Manibog *et al*., Molecular determinants of cadherin ideal bond formation: Conformation-dependent unbinding on a multidimensional landscape. *Proc. Natl. Acad. Sci. U.S.A.* **113**, E5711–E5720 (2016).
10. K. Manibog, H. Li, S. Rakshit, S. Sivasankar, Resolving the molecular mechanism of cadherin catch bond formation. *Nat. Commun.* **5**, 3941 (2014).
11. Y. Li *et al*., Mechanism of E-cadherin dimerization probed by NMR relaxation dispersion. *Proc. Natl. Acad. Sci. U.S.A.* **110**, 16462–16467 (2013).
12. A. Ratheesh, A. S. Yap, A bigger picture: Classical cadherins and the dynamic actin cytoskeleton. *Nat. Rev. Mol. Cell Biol.* **13**, 673–679 (2012).
13. S. Yonemura, Y. Wada, T. Watanabe, A. Nagafuchi, M. Shibata, alpha-Catenin as a tension transducer that induces adherens junction development. *Nat. Cell Biol.* **12**, 533–542 (2010).
14. T.-J. Kim *et al*., Dynamic visualization of α-catenin reveals rapid, reversible conformation switching between tension states. *Curr. Biol.* **25**, 218–224 (2015).
15. C. D. Buckley *et al*., Cell adhesion. The minimal cadherin-catenin complex binds to actin filaments under force. *Science* **346**, 1254211 (2014).
16. H.-J. Choi *et al*., αE-catenin is an autoinhibited molecule that coactivates vinculin. *Proc. Natl. Acad. Sci. U.S.A.* **109**, 8576–8581 (2012).
17. M. Yao *et al*., Force-dependent conformational switch of α-catenin controls vinculin binding. *Nat. Commun.* **5**, 1–12 (2014).
18. Q. le Duc *et al*., Vinculin potentiates E-cadherin mechanosensing and is recruited to actin-anchored sites within adherens junctions in a myosin II-dependent manner. *J. Cell Biol.* **189**, 1107–1115 (2010).
19. A. K. Barry *et al*., α-Catenin cytomechanics—Role in cadherin-dependent adhesion and mechanotransduction. *J. Cell Sci.* **127**, 1779–1791 (2014).
20. R. Seddiki *et al*., Force-dependent binding of vinculin to α-catenin regulates cell-cell contact stability and collective cell behavior. *Mol. Biol. Cell* **29**, 380–388 (2018).
21. W. A. Thomas *et al*., α-Catenin and vinculin cooperate to promote high E-cadherin-based adhesion strength. *J. Biol. Chem.* **288**, 4957–4969 (2013).
22. S. Huveneers, J. de Rooij, Mechanosensitive systems at the cadherin-F-actin interface. *J. Cell Sci.* **126**, 403–413 (2013).
23. D. E. Leckband, J. de Rooij, Cadherin adhesion and mechanotransduction. *Annu. Rev. Cell Dev. Biol.* **30**, 291–315 (2014).
24. R. M. Mège, N. Ishiyama, Integration of cadherin adhesion and cytoskeleton at adherens junctions. *Cold Spring Harb. Perspect. Biol.* **9**, a028738 (2017).
25. Ortega, F. E. *et al*. Adhesion to the host cell surface is sufficient to mediate Listeria monocytogenes entry into epithelial cells. *Mol. Biol. Cell*, **28**, 2945-2957 (2017).
26. F. Twiss *et al*., Vinculin-dependent Cadherin mechanosensing regulates efficient epithelial barrier formation. *Biol. Open* **1**, 1128–1140 (2012).
27. R. M. Hochmuth, E. A. Evans, Extensional flow of erythrocyte membrane from cell body to elastic tether. I. Analysis. *Biophys. J.* **39**, 71–81 (1982).
28. R. M. Hochmuth, H. C. Wiles, E. A. Evans, J. T. McCown, Extensional flow of erythrocyte membrane from cell body to elastic tether. II. Experiment. *Biophys. J.* **39**, 83–89 (1982).
29. E. Evans, V. Heinrich, A. Leung, K. Kinoshita, Nano- to microscale dynamics of P-selectin detachment from leukocyte interfaces. I. Membrane separation from the cytoskeleton. *Biophys. J.* **88**, 2288–2298 (2005).
30. E. Sariisik *et al*., Decoding cytoskeleton-anchored and non-anchored receptors from single-cell adhesion force data. *Biophys. J.* **109**, 1330–1333 (2015).
31. J. Schmitz, M. Benoit, K.-E. Gottschalk, The viscoelasticity of membrane tethers and its importance for cell adhesion. *Biophys. J.* **95**, 1448–1459 (2008).
32. V. Heinrich, A. Leung, E. Evans, Nano- to microscale dynamics of P-selectin detachment from leukocyte interfaces. II. Tether flow terminated by P-selectin dissociation from PSGL-1. *Biophys. J.* **88**, 2299–2308 (2005).
33. D. L. Rimm, E. R. Koslov, P. Kebriaei, C. D. Cianci, J. S. Morrow, Alpha 1(E)-catenin is an actin-binding and -bundling protein mediating the attachment of F-actin to the membrane adhesion complex. *Proc. Natl. Acad. Sci. U.S.A.* **92**, 8813–8817 (1995).
34. R. Desai *et al*., Monomeric α-catenin links cadherin to the actin cytoskeleton. *Nat. Cell Biol.* **15**, 261–273 (2013).
35. S. Huveneers *et al*., Vinculin associates with endothelial VE-cadherin junctions to control force-dependent remodeling. *J. Cell Biol.* **196**, 641–652 (2012).
36. Y. Sako, A. Nagafuchi, S. Tsukita, M. Takeichi, A. Kusumi, Cytoplasmic regulation of the movement of E-cadherin on the free cell surface as studied by optical tweezers and single particle tracking: Corralling and tethering by the membrane skeleton. *J. Cell Biol.* **140**, 1227–1240 (1998).
37. E. Evans, K. Ritchie, Dynamic strength of molecular adhesion bonds. *Biophys. J.* **72**, 1541–1555 (1997).
38. P. Panorchan *et al*., Single-molecule analysis of cadherin-mediated cell-cell adhesion. *J. Cell Sci.* **119**, 66–74 (2006).
39. Q. Shi, V. Maruthamuthu, F. Li, D. Leckband, Allosteric cross talk between cadherin extracellular domains. *Biophys. J.* **99**, 95–104 (2010).
40. N. Shashikanth *et al*., Allosteric regulation of E-cadherin adhesion. *J. Biol. Chem.* **290**, 21749–21761 (2015).
41. N. Shashikanth, M. A. Kisting, D. E. Leckband, Kinetic measurements reveal enhanced protein-protein interactions at intercellular junctions. *Sci. Rep.* **6**, 1–12 (2016).
42. S. Bunse *et al*., Role of N-cadherin cis and trans interfaces in the dynamics of adherens junctions in living cells. *PLoS One* **8**, e81517 (2013).
43. M. Krieg, J. Helenius, C. P. Heisenberg, D. J. Muller, A bond for a lifetime: Employing membrane nanotubes from living cells to determine receptor-ligand kinetics. *Angew. Chem. Int. Ed. Engl.* **47**, 9775–9777 (2008).
44. B. G. Hosu, M. Sun, F. Marga, M. Grandbois, G. Forgacs, Eukaryotic membrane tethers revisited using magnetic tweezers. *Phys. Biol.* **4**, 67–78 (2007).
45. G. I. Bell, Models for the specific adhesion of cells to cells. *Science* **200**, 618–627 (1978).
46. S. Chakrabarti, M. Hinczewski, D. Thirumalai, Plasticity of hydrogen bond networks regulates mechanochemistry of cell adhesion complexes. *Proc. Natl. Acad. Sci. U.S.A.* **111**, 9048–9053 (2014).
47. N. Borghi *et al*., E-cadherin is under constitutive actomyosin-generated tension that is increased at cell-cell contacts upon externally applied stretch. *Proc. Natl. Acad. Sci. U.S.A.* **109**, 12568–12573 (2012).
48. M. Kim, C. V. Carman, T. A. Springer, Bidirectional transmembrane signaling by cytoplasmic domain separation in integrins. *Science* **301**, 1720–1725 (2003).
49. S. Bajpai *et al*., alpha-Catenin mediates initial E-cadherin-dependent cell-cell recognition and subsequent bond strengthening. *Proc. Natl. Acad. Sci. U.S.A.* **105**, 18331–18336 (2008).
50. S. Bajpai, Y. Feng, R. Krishnamurthy, G. D. Longmore, D. Wirtz, Loss of α-catenin decreases the strength of single E-cadherin bonds between human cancer cells. *J. Biol. Chem.* **284**, 18252–18259 (2009).
51. I. Indra *et al*., Spatial and temporal organization of cadherin in punctate adherens junctions. *Proc. Natl. Acad. Sci. U.S.A.* **115**, E4406–E4415 (2018).
52. Y. Wu, P. Kanchanawong, R. Zaidel-Bar, Actin-delimited adhesion-independent clustering of E-cadherin forms the nanoscale building blocks of adherens junctions. *Dev. Cell* **32**, 139–154 (2015).
53. C. Bertocchi *et al*., Nanoscale architecture of cadherin-based cell adhesions. *Nat. Cell Biol.* **19**, 28–37 (2017).

54. J. A. Tunggal *et al*., E-cadherin is essential for in vivo epidermal barrier function by regulating tight junctions. *EMBO J.* **24**, 1146–1156 (2005).
55. O. Shafraz *et al*., E-cadherin binds to desmoglein to facilitate desmosome assembly. *eLife* **7**, e37629 (2018).
56. O. Shafraz, B. Xie, S. Yamada, S. Sivasankar, Mapping transmembrane binding partners for E-cadherin ectodomains. *Proc. Natl. Acad. Sci. U.S.A.* **117**, 31157–31165 (2020).
57. M. Sargiacomo, M. Lisanti, L. Graeve, A. Le Bivic, E. Rodriguez-Boulan, Integral and peripheral protein composition of the apical and basolateral membrane domains in MDCK cells. *J. Membr. Biol.* **107**, 277–286 (1989).
58. P. S. Caceres, D. Gravotta, P. J. Zager, N. Dephoure, E. Rodriguez-Boulan, Quantitative proteomics of MDCK cells identify unrecognized roles of clathrin adaptor AP-1 in polarized distribution of surface proteins. *Proc. Natl. Acad. Sci. U.S.A.* **116**, 11796–11805 (2019).
59. X. Peng, L. E. Cuff, C. D. Lawton, K. A. DeMali, Vinculin regulates cell-surface E-cadherin expression by binding to β-catenin. *J. Cell Sci.* **123**, 567–577 (2010).
60. C. Bertocchi, A. Ravasio, H. T. Ong, Y. Toyama, P. Kanchanawong, Mechanical roles of vinculin/β-catenin interaction in adherens junction. *BioRxiv* [Preprint] (2019). https://www.biorxiv.org/content/10.1101/770735v1.full (Accessed 23 September 2019).
61. A. Nagafuchi, S. Ishihara, S. Tsukita, The roles of catenins in the cadherin-mediated cell adhesion: Functional analysis of E-cadherin-alpha catenin fusion molecules. *J. Cell Biol.* **127**, 235–245 (1994).
62. Y. I. Petrova, M. M. Spano, B. M. Gumbiner, Conformational epitopes at cadherin calcium-binding sites and p120-catenin phosphorylation regulate cell adhesion. *Mol. Biol. Cell* **23**, 2092–2108 (2012).
63. S. L. Maiden, Y. I. Petrova, B. M. Gumbiner, Microtubules inhibit E-cadherin adhesive activity by maintaining phosphorylated p120-catenin in a colon carcinoma cell model. *PLoS One* **11**, e0148574 (2016).
64. Y. I. Petrova, L. Schecterson, B. M. Gumbiner, Roles for E-cadherin cell surface regulation in cancer. *Mol. Biol. Cell* **27**, 3233–3244 (2016).
65. T. Li *et al*., Loss of vinculin and membrane-bound β-catenin promotes metastasis and predicts poor prognosis in colorectal cancer. *Mol. Cancer* **13**, 263 (2014).
66. J. L. Rodríguez Fernández *et al*., Suppression of tumorigenicity in transformed cells after transfection with vinculin cDNA. *J. Cell Biol.* **119**, 427–438 (1992).
67. Y. Zhang, S. Sivasankar, W. J. Nelson, S. Chu, Resolving cadherin interactions and binding cooperativity at the single-molecule level. *Proc. Natl. Acad. Sci. U.S.A.* **106**, 109–114 (2009).
68. P. A. Longo, J. M. Kavran, M.-S. Kim, D. J. Leahy, Transient mammalian cell transfection with polyethylenimine (PEI). *Methods Enzymol.* **529**, 227–240 (2013).
69. J. L. Hutter, J. Bechhoefer, Calibration of atomic-force microscope tips. *Rev. Sci. Instrum.* **64**, 1868–1873 (1993).
70. C.-F. Yen, S. Sivasankar, Improving estimation of kinetic parameters in dynamic force spectroscopy using cluster analysis. *J. Chem. Phys.* **148**, 123301 (2018).